Article

Disorder-to-Order Transition of an Active-Site Loop Mediates the Allosteric Activation of Sortase A

Xiaodong Pang[1] and Huan-Xiang Zhou[1,*]
[1]Department of Physics and Institute of Molecular Biophysics, Florida State University, Tallahassee, Florida

ABSTRACT   Intrinsically disordered proteins and intrinsically disordered regions are implicated in many biological functions and associated with many diseases, but their conformational characterizations are challenging. The disordered $\beta6/\beta7$ loop of *Staphylococcus aureus* sortase A is involved in the binding of both sorting signals and calcium. Calcium binding allosterically activates the enzyme, but the detailed mechanism has been unclear. Here we adapted the replica exchange with solute tempering method to sample the conformations of the $\beta6/\beta7$ loop, in apo form and in three liganded forms (bound with a sorting signal or calcium or both). The extensive molecular dynamics simulations yield atomic details of the disordered-to-order transition of the loop and suggest a mechanism for allosteric activation: calcium binding results in partial closure and ordering of the loop, thereby leading to preorganization of the binding pocket for the sorting signal. The approach has general applicability to the study of intrinsically disordered regions.

INTRODUCTION

Intrinsically disordered proteins (IDPs) and intrinsically disordered regions (IDRs) are implicated in many biological functions including signaling and regulation, and associated with many diseases (1–3). The structure and function of IDPs and IDRs are receiving ever-increasing attention (4,5). In their functional processes, many IDPs and IDRs gain well-defined structures upon binding targets or ligands, often following a dock-and-coalesce mechanism (6). Conformational characterizations of IDPs and IDRs are a key step toward understanding functions and mechanisms. Here we report the adaption of a molecular dynamics simulation method called replica exchange with solute tempering (REST), to sample the conformations of an intrinsically disordered active-site loop of an enzyme, *Staphylococcus aureus* sortase A (SrtA).

SrtA anchors to proteins that bear a cell-wall sorting signal LPXTG (X representing any amino acid). A part of this process involves cleavage of the peptide bond between the Thr and Gly residues, and subsequent formation of a thioester bond between the SrtA catalytic residue Cys^{184} and the sorting signal Thr residue (7). As shown by nuclear magnetic resonance (NMR) and x-ray structures, the catalytic domain of SrtA (residues 60–206) adopts an eight-strand β-barrel fold (Fig. 1) (8–10). The sorting signal sits on a floor formed by residues around the termini of the $\beta4$, $\beta7$, and $\beta8$ strands and is enclosed by residues in the N-terminal region of the long $\beta6/\beta7$ loop (Fig. 1, B and C) (8,9). In the apo form, residues in this active-site loop showed exceedingly low NMR order parameters (11) as well as missing electron densities

and large conformational differences between subunits within the crystallographic asymmetric unit (9), suggesting structure disorder (Fig. 1 E). Ca^{2+} binding was found to increase the enzymatic activity by eightfold (10). The Ca^{2+} binding site is formed by residues in the $\beta3/\beta4$ loop and in the C-terminal region of the active-site loop, and hence is distal to the active site (Fig. 1, B and D) (8,10,11). Ca^{2+} binding quenched the fast (picoseconds to nanoseconds) dynamics of the active-site loop and redistributed slow (microseconds to milliseconds) dynamics toward the active site (11), but a detailed mechanism for the allosteric activation by Ca^{2+} is still lacking.

Conformational characterizations of IDPs and IDRs present a significant challenge for both experimental and computational approaches. Among the most useful experimental techniques, NMR spectroscopy can provide valuable but nevertheless limited data (12). Molecular dynamics simulations hold great potential, and a number of enhanced sampling methods have been applied to the study of IDPs and IDRs. For example, accelerated molecular dynamics simulations of SrtA by Kappel et al. (13) identified multiple possible binding modes for a substrate peptide. Temperature replica exchange molecular dynamics (14) has also been used to sample conformations of IDPs and IDRs (15,16). As the system size increases, the number of replicas required for adequate sampling becomes a limiting factor. As an alternative, Hamiltonian replica exchange methods have been developed. Among them, a method called multiscale enhanced sampling (MSES) was used to study the disorder-to-order transition of the SrtA active-site loop (17). The basic idea of MSES is that an all-atom representation of the system is coupled to a coarse-grained model and replicas with different coupling strengths are allowed
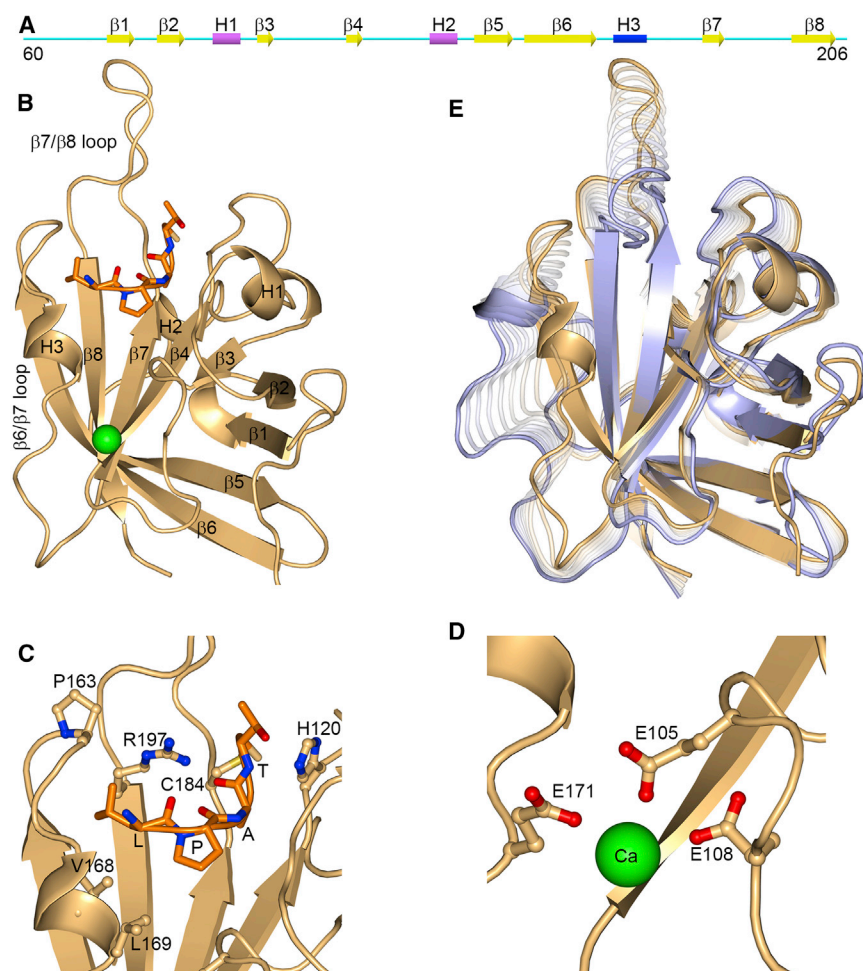
FIGURE 1 Structure of *S. aureus* sortase A. (*A*) Secondary structure of the catalytic domain. (*B*) The catalytic domain (colored in *gold*) bound with a sorting signal (sequence LPAT; in *orange*) and a Ca^{2+} ion (as *green sphere*), from model 1 of the NMR structure in PDB: 2KID (8). (*C*) Enlarged view of sorting signal binding site, displaying (as *ball-and-stick*) sorting signal-contacting residues around the C-termini of $\beta 4$ and $\beta 7$ and N-terminus of $\beta 8$ and in the N-terminal region of the active site (i.e., $\beta 6/\beta 7$) loop. (*D*) Enlarged view of the Ca^{2+} binding site, displaying (as *ball-and-stick*) the three glutamates that coordinate the Ca^{2+} ion. (*E*) Superposition of the x-ray structure for apo SrtA (chain C in PDB: 1T2P, *blue*) (9) and the NMR structure for SrtA$_{Pep/Ca}$ (*gold*). Conformational changes from apo to holo, especially prominent in the active-site loop (residues 159–177) and $\beta 7/\beta 8$ loop (residues 182–198), are illustrated by morphing calculated by the Yale Morph Server (36). The active-site loop in apo SrtA also exhibits significant structure disorder, as demonstrated by missing electron densities in chain B and large conformational differences between chains A and C (9). To see this figure in color, go online.

to exchange. The sampling efficiency is dictated by the ability of the coarse-grained simulations to capture the conformational dynamics of the all-atom model (18). MSES simulations found little effect on the conformations of the N-terminal region of the active-site loop by Ca^{2+} binding (17).

REST is a different form of Hamiltonian replica exchange, introduced by Liu et al. (19) and subsequently modified to improve sampling efficiency (20,21). An implementation in GROMACS is now available (21,22). In REST, the total potential energy of a system is divided into three components: the protein energy U_{pp}, the protein-solvent interaction energy U_{pw}, and the solvent energy U_{ww}. Scaling is introduced as

$$U_{REST} = \lambda U_{pp} + \sqrt{\lambda} U_{pw} + U_{ww},$$

and replicas are assigned a range of scaling factors with an upper bound of 1. Although all the replicas are simulated at the same temperature (T), with the scaling the effective temperature of the protein can be higher (at T/λ). By limiting the scaling to the first two energy terms, the exchange probability between two replicas is only determined by the energy of the protein and its interaction with the solvent, not by the energy of the large number of solvent molecules. Because the first two terms generally account for only a small percentage of the total energy of the system, a relatively small number of replicas is needed. REST has been used mostly for simulating folding and for conformational sampling of peptides (19–23), but also for conformational sampling of lipids in a bilayer (24) and of a ligand in a protein-ligand complex (25).

Normally a whole solute molecule (e.g., a peptide) is chosen for scaling. However, a region of a large solute molecule (e.g., a protein) can be just as well chosen to achieve enhanced sampling, and this choice is a perfect match for exploring the conformational ensembles of IDRs. Here we used this REST protocol to investigate the disorder-to-order transition of the SrtA active-site loop. We demonstrate significant gain in sampling efficiency over a conventional molecular dynamics (cMD) simulation and arguably also gain over the previous MSES simulations. In our REST simulation on apo SrtA, the active-site loop exhibits considerable flexibility, as evidenced by the coexistence of three

conformational substates. Binding of either a sorting signal or Ca^{2+} or both reduces the flexibility of the active-site loop, now largely confined to a single conformational state. Importantly, the simulations show that binding of Ca^{2+} alone induces partial closure and ordering of the active-site loop, thereby leading to preorganization of the binding pocket for the sorting signal. That is, prebinding of Ca^{2+} with the $\beta3/\beta4$ loop accelerates the docking of the C-terminal region of the active-site loop via electrostatic attraction, and furthermore facilitates the coalescence of the N-terminal region of this loop around the sorting signal.

MATERIALS AND METHODS

System and simulation setup

The starting structure for simulations on apo SrtA was model 1 of the NMR structure of Ca^{2+}-bound SrtA (SrtA$_{Ca}$; PDB: 1IJA), in which Ca^{2+} was missing due to lack of structural restraints. The starting structures for simulations on the three liganded forms were all from model 1 of the NMR structure of holo SrtA (SrtA$_{Pep/Ca}$; PDB: 2KID), with either the sorting signal (sequence LPAT) or the Ca^{2+} ion or both retained. The sorting signal was capped by acetyl and N-methyl amide groups, respectively, at the N- and C-termini. Similar to Moritsugu et al. [17], we weakly constrained the sorting signal and Ca^{2+} ion to their respective binding sites, by one-sided harmonic potentials. The harmonic potentials had a force constant of 0.5 kcal/mol/Å^2 and started at an interatomic distance of 5 Å for the sorting signal or 3.5 Å for the Ca^{2+} ion. For the sorting signal, the one-sided harmonic constraints were imposed on peptide-protein heavy atom pairs within a 4-Å distance cutoff in model 1 of 2KID, excluding the active-site loop (residues 159–177) and the $\beta7/\beta8$ loop (residues 182–198), but including the pair between the carbonyl oxygen of the peptide C-terminal threonine and the sulfur of the protein Cys^{184} (to mimic the thioester bond). For the Ca^{2+} ion, the constraint partners were the oxygen atoms in the side chains of Glu^{171}, Glu^{105}, Glu^{108}, and Asp^{112} and the backbone of Asn^{114}.

We performed five separate simulations using GROMACS 4.6.3 [26] patched with the PLUMED 2.0 plug-in [22]. One was a cMD simulation on apo SrtA, lasting 1600 ns. The other four were REST simulations on apo SrtA, SrtA$_{Ca}$, sorting signal-bound SrtA (SrtA$_{Pep}$), and SrtA$_{Pep/Ca}$. Each REST simulation involved 16 replicas and each replica was simulated to 100 ns; hence the total simulation time was also 1600 ns. The force field was Amber99sb [27]. The solvent between each protein system and the nearest side of the cubic simulation box was at least 10 Å thick, comprising ~9000 TIP3P water molecules and 0.15 M neutralizing NaCl. Long-range electrostatic interactions were treated using particle-mesh Ewald [28], with a direct-space cutoff of 10 Å and a grid spacing of 1.2 Å. Temperature was maintained at 300 K by velocity rescaling. All bonds involving hydrogen atoms were restrained by LINCS [29], allowing an integration time of 2 fs.

Details of REST protocol

The 19 residues of the active-site loop were selected for enhanced sampling. In the REST simulations, replica exchanges were attempted every 2 ps [20]. The values of the scaling factor λ were adjusted by trial and error to achieve roughly equal acceptance rates for exchanges between neighboring replicas. For each REST simulation, 16 replicas were used, and the λ-values finally chosen were: 1, 0.965, 0.930, 0.895, 0.860, 0.825, 0.790, 0.755, 0.721, 0.688, 0.656, 0.625, 0.595, 0.566, 0.538, and 0.511. Correspondingly, the effective temperatures (i.e., T/λ) of the active-site loop in the 16 replicas were 300, 311, 323, 335, 349, 364, 380, 397, 416, 436, 457, 480, 504, 530, 558, and 587 K. The acceptance rate was ~0.47.

Principal component analysis

Principal component analysis (PCA) was performed on conformations collected from all the five simulations and NMR and x-ray structures of SrtA. The total collection consisted of 50,000 conformations from the cMD simulation on apo SrtA, sampled at every 32 ps; 50,000 conformations from each of the four REST simulations, sampled on the replica with $\lambda = 1$ at every 2 ps; 25 models in the NMR structure of SrtA$_{Ca}$ (PDB: 1IJA); 20 models in the NMR structure of SrtA$_{Pep/Ca}$ (PDB: 2KID); and two chains in the x-ray structure of apo SrtA (PDB: 1T2P). Before PCA, all the conformations were superimposed on the $C\alpha$ atoms of the $\beta1$ (residues 74–78), $\beta2$ (residues 83−87), $\beta5$ (residues 141–146), and $\beta6$ (residues 149–156) strands. PCA on the $C\alpha$ atoms of the active-site loop used the built-in tools in GROMACS.

Chemical shift prediction

Backbone chemical shifts were predicted using the SPARTA+ program [30], on 2500 conformations from each REST simulation (sampled at every 40 ps). SPARTA+ was trained on a database of chemical shifts for structured proteins. Chemical shift predictions for the SrtA IDR could therefore be worse than for the structured regions.

RESULTS

We carried out extensive molecular dynamics simulations to explore the conformational ensembles of the SrtA active-site loop in the apo form and the three liganded forms. A long (1600-ns) cMD simulation on apo SrtA served as a benchmark for evaluating sampling efficiency. Four 100-ns REST simulations, each involving 16 replicas in which the potential energy of the active-site loop was scaled downward to different extents to mimic heating up to 587 K, were used to compare conformational preferences among apo SrtA, SrtA$_{Ca}$, SrtA$_{Pep}$, and SrtA$_{Pep/Ca}$.

REST versus cMD on apo SrtA

The cMD and REST simulations on apo SrtA accrued the same total simulation time (1600 ns) and started from the same structure, i.e., model 1 of the NMR structure for SrtA$_{Ca}$ (PDB: 1IJA) [10], in which Ca^{2+} was missing. The conformational space covered by the REST simulation is significantly broader than the cMD simulation (Fig. 2). To display the difference, we carried out PCA on the active-site loop after superposition on four β-strands (Fig. 2, A and B, *cyan ribbon*). The first two principal components, PC1 and PC2, capture global movements of the active-site loop (Fig. 2, A and B, *arrows*). These movements are largely confined to a plane parallel to the central β-sheet comprising $\beta4$, $\beta7$, and $\beta8$, and can thus be described as "gliding". PC1 is approximately directed at the sorting signal binding site whereas PC2 is approximately directed at the Ca^{2+} binding site. We obtained the distributions of PC1 and PC2 in the cMD and REST simulations and then converted them into free-energy surfaces according to the Boltzmann relation. In the cMD simulation the active-site loop is mostly in a semiopen substate, defined by a narrow free-energy basin
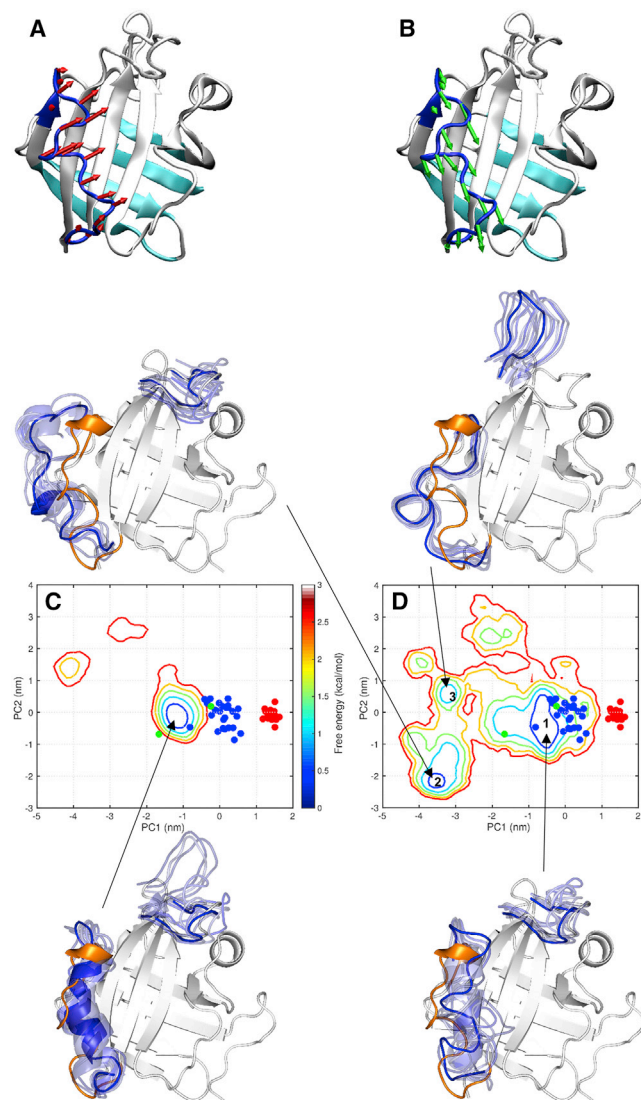
FIGURE 2 Comparison of conformational ensembles of apo SrtA sampled by the cMD and REST simulations. (*A* and *B*) Conformational differences represented by the first two principal components, PC1 (*red arrows*) and PC2 (*green arrows*), on a SrtA conformation with both PC1 and PC2 near 0. Four β-strands (*cyan*), $\beta 1$, $\beta 2$, $\beta 5$, and $\beta 6$, were used for superposition before PCA on the active-site loop. The view is rotated by ~45° around a vertical axis from that for Fig. 1. (*C* and *D*) Free-energy surfaces, calculated from distributions of PC1 and PC2 in the cMD and REST simulations, respectively, on apo SrtA and contoured at 0.5 kcal/mol internals. PC coordinates are also displayed for chains A and C in the x-ray structure of apo SrtA (PDB: 1T2P) (*green dots*); 25 models in the NMR structure of SrtA$_{Ca}$ (PDB: 1IJA) (*blue dots*); and 20 models in the NMR structure of SrtA$_{Pep/Ca}$ (PDB: 2KID) (*red dots*). One substate from the cMD simulation and three substates from the REST simulations are each illustrated by 10 conformations within the first contour around a free-energy local minimum, with only the active-site loop and $\beta 7/\beta 8$ loop displayed (in *blue*) along with chain C of 1T2P (*gray* with active-site loop in *orange*). To see this figure in color, go online.

bordered by the conformations of chains A and C in the x-ray structure for apo SrtA (PDB: 1T2P; Fig. 2 *C*) (9). The corresponding basin in the REST simulation is significantly broader, and contains both of the two x-ray confor-

mations for apo SrtA and the 25 NMR models for SrtA$_{Ca}$ (Fig. 2 *D*). Moreover, two other basins appear. Hereafter the conformational substates defined by the three free-energy basins will be numbered 1, 2, and 3, respectively. Whereas the active-site loop is semiopen in substate 1, it is wide open in the N-terminal region in substate 2, and wide open in the C-terminal region in substate 3. Below, we will use substate 1 of apo SrtA in the REST simulation as the reference for describing conformational changes in the liganded forms.

The apo x-ray structure and holo NMR structure show that residues in the active-site loop have a tendency to form a 3_{10} helix, but not an α-helix. This tendency is captured well by the REST simulation, showing 15% of average 3_{10} helix content for the active-site loop and little sign of α-helix. On the other hand, in the cMD simulation the active-site loop has a significant α-helix content (at 17%; see also Fig. 2 *C*). The propensity for a 3_{10} helix is also seen in the REST simulations on the three liganded forms (see Fig. S1 in the Supporting Material for residue-specific 3_{10} helix probabilities). A 3_{10} helix is present in the active-site loop of apo SrtA from *Streptococcus pyogenes* (31), which has 24% sequence identity with the *S. aureus* ortholog.

Besides the active-site loop, the $\beta 7/\beta 8$ loop also exhibits a significant conformational change from the apo x-ray structure to the holo NMR structure, opening up as if to make room for the bound sorting signal (Fig. 1 *E*). In the cMD simulation, the $\beta 7/\beta 8$ loop is sporadically open (Fig. 2 *C*). In the REST simulation, the $\beta 7/\beta 8$ loop is stably open in substate 3 (Fig. 2 *D*). Here the N-terminal region of the active-site loop has the closest approach to $\beta 8$, thereby mimicking an arriving sorting signal in pushing open the $\beta 7/\beta 8$ loop. The REST simulation thus was able to reveal an apparent cooperative effect between the active-site and $\beta 7/\beta 8$ loops, even though only one of them was subject to energy scaling for enhanced sampling.

Taken together, we can conclude that the REST simulation provides a much more extensive sampling of the conformational space of the active-site loop than the cMD simulation. The results below further suggest that REST may exceed MSES in sampling efficiency. The REST sampling efficiency came about because the replicas readily exchanged (Fig. S2). Regardless where along the effective temperature ladder a replica was started, it was able to traverse the entire ladder with significant probabilities during the simulations.

Disorder-to-order transition of the active-site loop upon ligand binding

The preceding REST simulation shows that in the apo form the active-site loop can readily exchange between three conformational substates, which together cover a broad area over PC1 and PC2. Upon binding of either Ca^{2+} or the sorting signal, and especially upon binding both, the

active-site loop significantly loses flexibility and becomes largely confined to a single conformational state (Fig. 3). Relative to substate 1 of apo SrtA (Fig. 2 D), the free-energy basins of the liganded forms all shift toward larger PC1, representing closure of the active-site loop. The merging and compaction of free-energy basins exposed by the REST simulations are the essence of the ligand-induced, disorder-to-order transition of the active-site loop.

To test for sampling convergence, we divided the 100-ns REST simulations into two equal segments and compared the results separately calculated from the conformations in the two segments (Fig. S3). Overall, the results from the two segments are very similar to each other and to those in Figs. 2 D and 3 for the entire series of 100-ns simulations. The major free-energy basins are matched well, although the two smaller basins for apo SrtA show some differences between the two simulation segments, with basin 2 being more prominently sampled in the first segment, and basin 3 being more so in the second segment. The convergence is not surprising given that, during the 100-ns simulations,
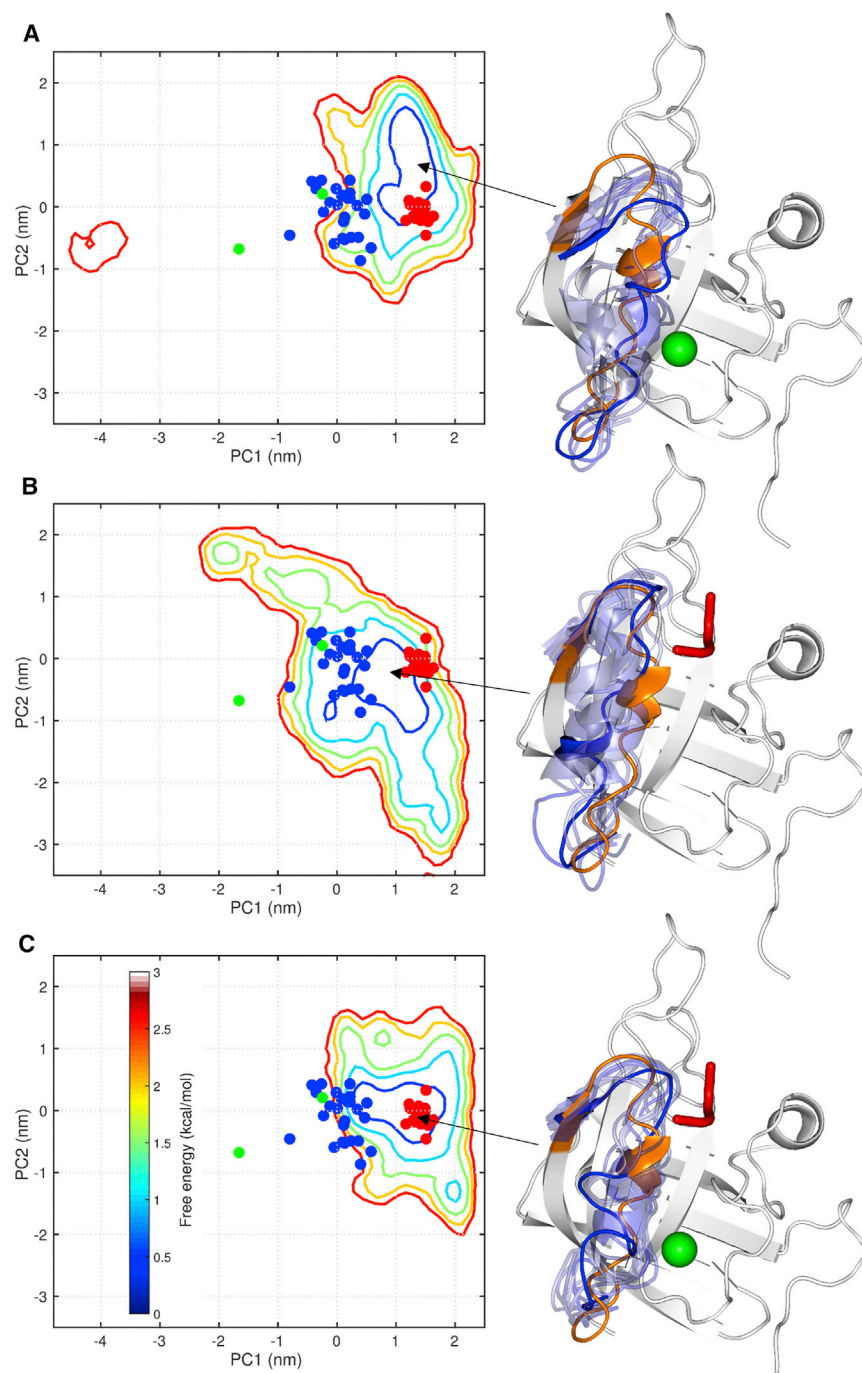

FIGURE 3 Conformational ensembles of SrtA in three liganded forms. (A) SrtA$_{Ca}$. (B) SrtA$_{Pep}$. (C) SrtA$_{Pep/Ca}$. The information presented is the same as in Fig. 2, C and D, except that the free-energy surfaces are calculated from the REST simulations on the three liganded forms. Each free-energy basin is illustrated by 10 conformations within the first contour (at 0.5 kcal/mol) around the minimum, with only the active-site loop displayed (in *blue*) along with model 1 of 2KID (*gray* with active-site loop in *orange*). To see this figure in color, go online.

each replica readily traversed the entire temperature ladder (Fig. S2).

The holo form has the most compact free-energy basin; the 20 NMR models for $SrtA_{Pep/Ca}$ are clustered around the free-energy minimum (Fig. 3 C). Relative to the apo substate 1, the active-site loop in the holo form is tightly closed, and maintains contact with both the sorting signal and Ca^{2+} (through the N-and C-terminal regions, respectively). In comparison, the free-energy basin of $SrtA_{Pep}$ is less compact, and at the free-energy minimum the active-site loop is closed not as tightly as in the holo form, but does maintain the N-terminal interaction with the sorting signal (Fig. 3 B). The vast majority of the $SrtA_{Ca}$ conformations are found in a very compact free-energy basin where the active-site loop is closed nearly as tightly as in $SrtA_{Pep/Ca}$ but does not reach far into the sorting signal binding site (Fig. 3 A). In a small minority of the $SrtA_{Ca}$ conformations, the active-site loop is wide open.

Calcium promotes sorting signal binding by preorganization of the binding pocket

The foregoing results provide direct support to the speculation of Naik et al. (11) that Ca^{2+} achieves allosteric activation by stabilizing closed conformations of the active-site loop poised for binding the sorting signal. These PCA results capture the global movements of the active-site loop. We now present detailed information on the formation of the binding pockets for Ca^{2+} and the sorting signal.

We used two distances, d_{Ca} and d_{Pep}, to indicate the formation of the two binding pockets. Their definitions are the same as those of Moritsugu et al. (17), to allow for easy comparison with the previous MSES simulations. Namely, d_{Ca} is the smaller of the $C\delta$-$C\delta$ distances from Glu^{171} to Glu^{105} and Glu^{108} (Fig. 1 D), whereas d_{Pep} is the $C\alpha$-$C\alpha$ distance from Pro^{163} to Arg^{197} (Fig. 1 C). The free-energy surfaces over d_{Pep} and d_{Ca} calculated from the REST simulations on apo SrtA and the three liganded forms are shown in Fig. 4. The free-energy surface for apo SrtA spreads over a broad area, with multiple local minima (Fig. 4 A). One cluster of minima corresponds to substate 1 defined above (featuring a semi-open active-site loop), with d_{Pep} averaging to ~7 Å; the other cluster encompasses substates 2 and 3, with d_{Pep} ranging from 10 to 17 Å (Fig. 4, A and E). In both clusters, the Ca^{2+} binding pocket is not formed, as indicated by a broad distribution in d_{Ca} (Fig. 4 F). The free-energy surface for $SrtA_{Pep}$ also covers a relatively broad area, with a major basin centered at d_{Pep} ~ 6 Å and d_{Ca} ~ 16 Å (Fig. 4 C). Again, the Ca^{2+} binding pocket is not formed, with a distribution in d_{Ca} similar to that in apo SrtA (Fig. 4 F). The absence of a well-formed Ca^{2+} binding pocket in both apo SrtA and $SrtA_{Pep}$ is understandable, as its presence would mean direct contact between like-charged Glu^{171} and Glu^{105}/Glu^{108}.

PC1 and d_{Pep} present two ways to describe the movement of the active-site loop relative to the sorting signal binding site. Not surprisingly, there is strong correlation between PC1 and d_{Pep} for apo SrtA, $SrtA_{Ca}$, and $SrtA_{Pep}$, with R^2 of linear regression at 0.78, 0.65, and 0.52, respectively. For $SrtA_{Pep/Ca}$, the correlation between PC1 and d_{Pep} becomes weak because of the restricted ranges of the sampled PC1 and d_{Pep} values in this case. Although both PC2 and d_{Ca} describe the movement of the active-site loop relative to the Ca^{2+} binding site, the former is defined with only $C\alpha$ positions whereas the latter is also dictated by significant side-chain motions, and hence their correlation is weak for all four systems.

Moritsugu et al. (17) presented free-energy surfaces over d_{Pep} and d_{Ca} from their MSES simulations on apo SrtA and $SrtA_{Pep}$. In both cases, when compared to the counterparts in the REST simulations, significantly smaller areas over d_{Pep} and d_{Ca} were covered, suggesting less extensive conformational sampling. In particular, d_{Pep} extended to 12 and 8 Å for apo SrtA and $SrtA_{Pep}$, respectively, in the MSES simulations, but to 17 and 13 Å in the REST simulations. The conformational characterizations of the holo form are more similar in the MSES and REST simulations.

Notably, for $SrtA_{Ca}$ our free-energy surface spans very limited regions over d_{Ca} and d_{Pep} (Fig. 4 B). The compact basin over PC1 and PC2 shown in Fig. 3 A is now characterized here by both short d_{Ca} (appropriate for Ca^{2+} coordination; Fig. 4 E) and a distribution in d_{Pep} sharply peaked at a low value (~5.5 Å), but with a right tail (Fig. 4 F). The short d_{Pep} in the vast majority of the conformations in this basin indicates that Ca^{2+} binding is accompanied by closure and ordering of the N-terminal region of the active-site loop, leading to preorganization of the binding pocket for the sorting signal. The right tail of the distribution in d_{Pep} shows that the N-terminal region (as represented by Pro^{163}) of the active-site loop in $SrtA_{Ca}$ can transiently open but strongly prefers the closed state, through interactions with the N-terminus (as represented by Arg^{197}) of $\beta 8$. In a second, minor free-energy basin, the N-terminal region of the active-site loop interacts with the N-terminus of $\beta 8$, but the C-terminal region of the active-site loop loses coordination with the bound Ca^{2+}, with the side chain of Glu^{171} pointing outward and thus resulting in long d_{Ca}. Overall, the extent of closure and ordering of the active-site loop in $SrtA_{Ca}$ nearly approaches that in $SrtA_{Pep/Ca}$ (Fig. 4, B and D–F). In contrast, the MSES simulation on $SrtA_{Ca}$ by Moritsugu et al. (17) found Ca^{2+}-induced formation of the sorting signal binding pocket to be "limited to a small range", as shown by a broad distribution in d_{Pep} that was only slightly left-shifted from the counterpart for apo SrtA.

The values of d_{Pep} and d_{Ca} map the two chains of the apo x-ray structure to the center of the major free-energy basin for apo SrtA (Fig. 4 A) and the 20 models of the holo NMR structure to the center of the major free-energy basin for $SrtA_{Pep/Ca}$ (Fig. 4 D). However, only model 1 of the 25 models
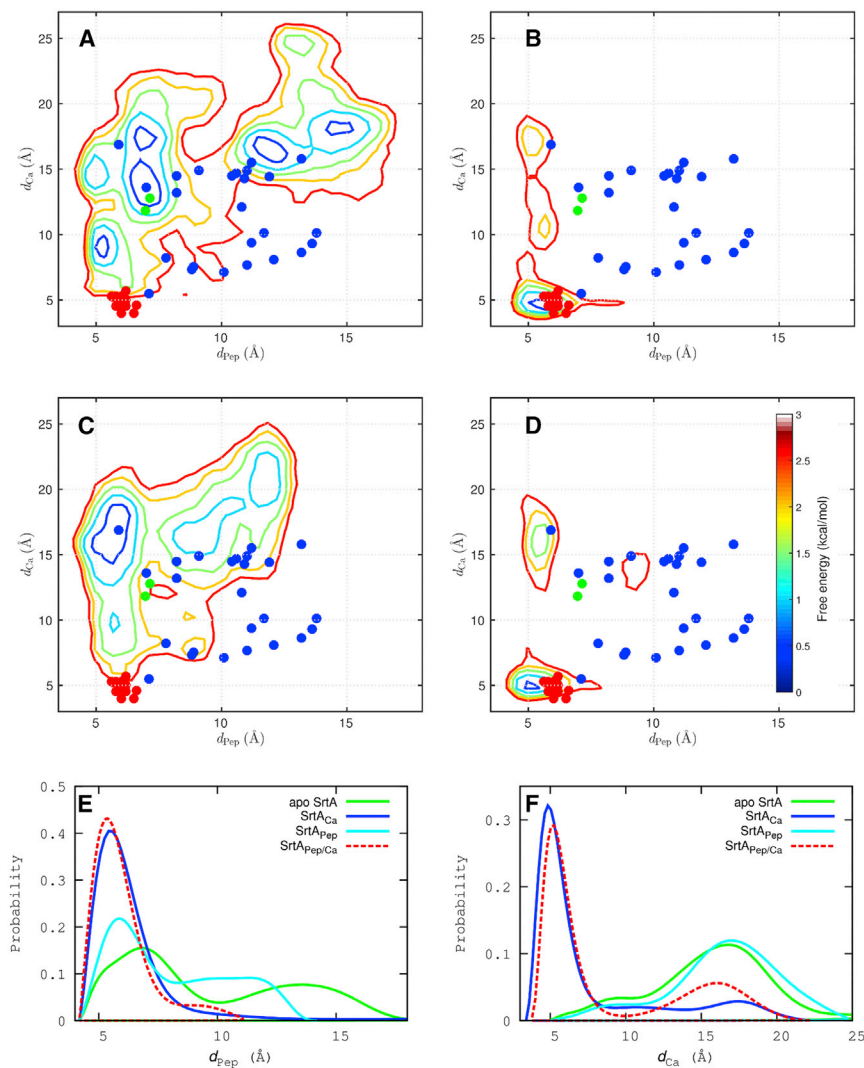
FIGURE 4 Status of sorting signal and Ca^{2+} binding pockets, monitored by d_{Pep} and d_{Ca}, respectively. (*A–D*) Free-energy surfaces over d_{Pep} and d_{Ca} for apo SrtA, SrtA$_{Ca}$, SrtA$_{Pep}$, and SrtA$_{Pep/Ca}$, respectively, contoured at 0.5 kcal/mol internals. The d_{Pep} and d_{Ca} values are also displayed for conformations in 1T2P (*green dots*); 1IJA (*blue dots*); and 2KID (*red dots*). (*E* and *F*) Distributions of d_{Pep} and d_{Ca}, respectively. To see this figure in color, go online.

in the NMR structure for Ca^{2+}-bound SrtA is located within the major free-energy basin for SrtA$_{Ca}$ (Fig. 4 *B*). That the other 24 models show significant scatter in both d_{Pep} and d_{Ca} is largely a reflection of the paucity of structural restraints on the active-site loop (especially side chains therein) due to resonance overlap and line-broadening (10).

The considerable increase in structure order shown in our simulation on SrtA$_{Ca}$ is consistent with the Ca^{2+}-induced quenching of picosecond motions within the active-site loop indicated by NMR spectroscopy (10). Quenching of fast (picosecond-nanosecond) motions, along with initiation of slow (microsecond-millisecond) motions, appears to be a common phenomenon for allosteric activators (32). To obtain further validation of our simulations, we calculated $C\alpha$ chemical shifts on the sampled conformations of SrtA$_{Ca}$ and apo SrtA and compared the resulting chemical shift perturbations to the data presented by Ilangovan et al. (10). As shown in Fig. S4, the calculated chemical shift perturbations are qualitatively similar to the experimental data, with large

values for the $\beta3/\beta4$ loop and the active-site loop. Moreover, the occasional long d_{Pep} sampled by SrtA$_{Ca}$ may explain the significant line-broadening observed on some residues in the N-terminal region of the active-site loop, and the occasional long d_{Ca} may be consistent with residual picosecond motions in the C-terminal region in the presence of Ca^{2+} (10).

DISCUSSION

We have adapted the REST method to carry out extensive simulations on SrtA in the apo form and in three liganded forms. Compared to conventional molecular dynamics simulation and even possibly to the MSES method, REST significantly enhances the sampling efficiency. The simulations show that the ligand-induced disorder-to-order transition of the active-site loop is characterized by merging and compaction of free-energy basins. Calcium binding leads to the preorganization of the binding pocket for sorting signals, but not vice versa.

Mechanism of allosteric activation

Our simulation results delineate a detailed mechanism for the allosteric activation of SrtA by Ca^{2+} (Fig. 5). In apo SrtA, the active-site loop undergoes conformational exchange among three substates, one that is semiopen and two that are wide open; the $\beta 7/\beta 8$ loop is closed most of the time, but tends to open when the N-terminal region of the active-site loop encroaches. When the sorting signal binds, the $\beta 7/\beta 8$ loop opens up to make room, and the active-site loop has the N-terminal region enclosing the peptide but the C-terminal region remaining open to avoid charge-charge repulsion by anionic residues including Glu^{105} and Glu^{108}. When Ca^{2+} binds, the entire active-site loop closes up, stabilized by interactions between Glu^{171} and the prebound Ca^{2+} and between the N-terminal region and the $\beta 8$ N-terminus. The latter interaction increases the tendency of the $\beta 7/\beta 8$ loop to open, preorganizing the binding pocket for the sorting signal. When the sorting signal then comes in for binding, the binding pocket just needs to make fine adjustments, including the upshift of the N-terminal region of the active-site loop.

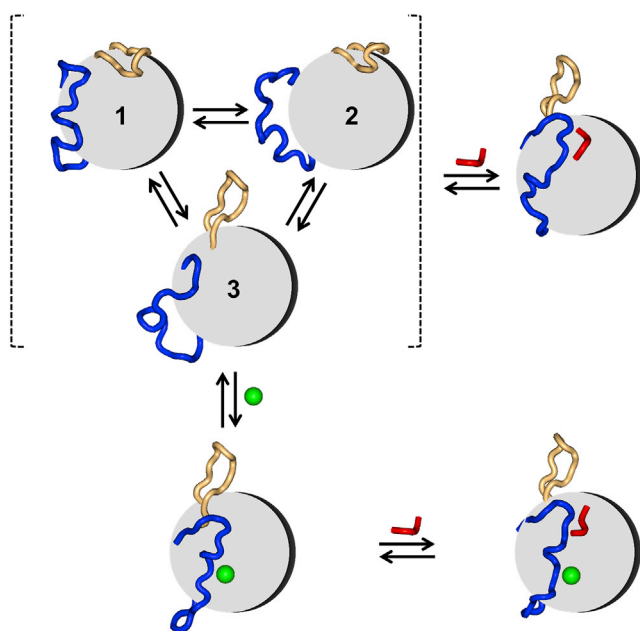In this allosteric mechanism, the active-site loop plays a critical role. The conformational heterogeneity exhibited by the active-site loop in the apo form persists to a large degree when the sorting signal is bound without Ca^{2+}, especially in the C-terminal region but also in the N-terminal region. Here, the N-terminal region of the active-site loop therefore does not strongly contribute to the proper positioning and/or binding stability of the sorting signal, leading to the relatively low enzymatic activity of the Ca^{2+}-free enzyme. When Ca^{2+} is bound, the active-site loop, through partial closure and ordering, appears to be the main conduit for the allosteric communication from the Ca^{2+} binding site to the active site.

Based on our other studies on the binding of IDPs to structured targets (6), we can further speculate a possible pathway for the allosteric communication. Initially the prebound Ca^{2+} might, through long-range electrostatic attraction, recruit Glu^{171} for coordination, leading to the docking of the C-terminal region of the active-site loop. Thereafter the N-terminal region would look for interaction partners and eventually coalesce around the $\beta 8$ N-terminus (and the sorting signal when present). The *S. pyogenes* SrtA is Ca^{2+}-insensitive and there a cationic residue, Lys^{126}, substitutes for the *S. aureus* Glu^{105} (31). Interestingly, Lys^{126} may serve a role similar to that of Ca^{2+}. It forms a salt bridge with Asp^{196} (corresponding to *S. aureus* Glu^{171}) on the active-site loop, and this interaction may initiate the dock-and-coalesce pathway just outlined for the Ca^{2+}-loaded *S. aureus* SrtA.

If the allosteric mechanism outlined here is correct, then an E105K mutation of *S. aureus* SrtA may allow the protein in apo form to reach the catalytic activity of the Ca^{2+}-loaded form of the wild-type protein, because the anticipated salt bridge with Glu^{171} may elicit a similar allosteric effect to Ca^{2+} binding. It will be interesting to test the catalytic activities of this type of mutant.

FIGURE 5 Mechanistic model for allosteric activation of SrtA by Ca^{2+}. β-barrel of SrtA (*gray*), active-site loop (*blue*), $\beta 7/\beta 8$ loop (*orange*), sorting signal (*red*), and Ca^{2+} (*green*). In the apo form, the active-site loop undergoes conformational exchange among three substates, and the $\beta 7/\beta 8$ loop is mostly closed but can transiently open. Upon binding of the sorting signal, the active-site loop closes up but retains significant mobility, partly due to repulsion of Glu^{171} by anionic residues such as Glu^{105} and Glu^{108}. The Ca^{2+} binding leads to closure of the entire active-site loop and increased open probability for the $\beta 7/\beta 8$ loop. The resulting preorganization of the binding pocket for the sorting signal facilitates the latter's tight binding. To see this figure in color, go online.

General use of REST for simulations on IDRs

Our study demonstrates that the REST method is ideally suited for efficient conformational sampling of IDRs. With SrtA solvated in explicit solvent, only 16 replicas were needed to cover an effective temperature range from 300 to nearly 600 K, at an acceptance rate of ~0.47 for replica exchange. Using the traditional temperature replica exchange, to achieve the coverage of the same temperature at the same acceptance rate would require as many as 200 replicas (33). Our simulations also appear to be more efficient than simulations for the same SrtA systems using MSES, which like REST is also a form of Hamiltonian replica exchange. Specifically, our simulations yielded broader coverage of the conformational space for the active-site loop in apo SrtA and in SrtA$_{Pep}$. More importantly, our simulations presented direct evidence for the allosteric activation of SrtA by Ca^{2+}, in the form of closure and ordering of the entire active-site loop and the consequent preorganization of the binding site for the sorting

signal. In contrast, Moritsugu et al. (17) concluded that Ca^{2+} binding had little effect on the N-terminal region of the active-site loop. The apparently more limited sampling by MSES may be a reflection of the intrinsic ability of this method, or may be due to artificial bias in the choice of the coarse-grained model. The use of two versions of the Amber force field (Amber99sb here and Amber03 in the MSES study, differing in backbone torsion parameters and partial charges) could conceivably result in a difference in sampling efficiency. A rigorous comparison of the sampling efficiencies of REST and MSES will require extensive simulations using the same force field, best done on test systems much smaller than SrtA.

IDRs/IDPs are implicated in many biological functions and often associated with diseases. Designing drugs for disordered proteins is a challenge due to the conformational heterogeneity. A critical step is to better understand the binding mechanisms and disorder-to-order transitions of disordered proteins, particularly the motifs involved in ligand recognition. SrtA itself is an ideal drug target (34,35). The types of conformational substates and binding and allosteric mechanisms revealed by REST simulations may guide drug discovery in the future. While for SrtA the IDR selected for enhanced sampling appears to contain most of the allosteric pathway, in other cases allosteric pathways may not be largely confined to isolated, small IDRs. Finding the balance between optimizing sampling efficiency and maximizing the coverage of the allosteric pathways will be a challenge for future studies.

SUPPORTING MATERIAL

Four figures are available at http://www.biophysj.org/biophysj/supplemental/S0006-3495(15)00921-2.

AUTHOR CONTRIBUTIONS

X.P. and H.-X.Z. designed the research; X.P. performed the research and analyzed the data; and X.P. and H.-X.Z. wrote the article.

ACKNOWLEDGMENTS

REFERENCES

1. Dunker, A. K., J. D. Lawson, …, Z. Obradovic. 2001. Intrinsically disordered protein. *J. Mol. Graph. Model.* 19:26–59.

2. Babu, M. M., R. van der Lee, …, J. Gsponer. 2011. Intrinsically disordered proteins: regulation and disease. *Curr. Opin. Struct. Biol.* 21:432–440.

3. Wright, P. E., and H. J. Dyson. 2015. Intrinsically disordered proteins in cellular signalling and regulation. *Nat. Rev. Mol. Cell Biol.* 16:18–29.

4. Oldfield, C. J., and A. K. Dunker. 2014. Intrinsically disordered proteins and intrinsically disordered protein regions. *Annu. Rev. Biochem.* 83:553–584.

5. Uversky, V. N. 2014. Introduction to intrinsically disordered proteins (IDPs). *Chem. Rev.* 114:6557–6560.

6. Zhou, H. X., X. Pang, and C. Lu. 2012. Rate constants and mechanisms of intrinsically disordered proteins binding to structured targets. *Phys. Chem. Chem. Phys.* 14:10466–10476.

7. Ton-That, H., G. Liu, …, O. Schneewind. 1999. Purification and characterization of sortase, the transpeptidase that cleaves surface proteins of *Staphylococcus aureus* at the LPXTG motif. *Proc. Natl. Acad. Sci. USA.* 96:12424–12429.

8. Suree, N., C. K. Liew, …, R. T. Clubb. 2009. The structure of the *Staphylococcus aureus* sortase-substrate complex reveals how the universally conserved LPXTG sorting signal is recognized. *J. Biol. Chem.* 284:24465–24477.

9. Zong, Y., T. W. Bice, …, S. V. L. Narayana. 2004. Crystal structures of *Staphylococcus aureus* sortase A and its substrate complex. *J. Biol. Chem.* 279:31383–31389.

10. Ilangovan, U., H. Ton-That, …, R. T. Clubb. 2001. Structure of sortase, the transpeptidase that anchors proteins to the cell wall of *Staphylococcus aureus*. *Proc. Natl. Acad. Sci. USA.* 98:6056–6061.

11. Naik, M. T., N. Suree, …, R. T. Clubb. 2006. *Staphylococcus aureus* Sortase A transpeptidase. Calcium promotes sorting signal binding by altering the mobility and structure of an active site loop. *J. Biol. Chem.* 281:1817–1826.

12. Jensen, M. R., R. W. H. Ruigrok, and M. Blackledge. 2013. Describing intrinsically disordered proteins at atomic resolution by NMR. *Curr. Opin. Struct. Biol.* 23:426–435.

13. Kappel, K., J. Wereszczynski, …, J. A. McCammon. 2012. The binding mechanism, multiple binding modes, and allosteric regulation of *Staphylococcus aureus* Sortase A probed by molecular dynamics simulations. *Protein Sci.* 21:1858–1871.

14. Sugita, Y., and Y. Okamoto. 1999. Replica-exchange molecular dynamics method for protein folding. *Chem. Phys. Lett.* 314:141–151.

15. Zhang, W., D. Ganguly, and J. Chen. 2012. Residual structures, conformational fluctuations, and electrostatic interactions in the synergistic folding of two intrinsically disordered proteins. *PLOS Comput. Biol.* 8:e1002353.

16. Knott, M., and R. B. Best. 2012. A preformed binding interface in the unbound ensemble of an intrinsically disordered protein: evidence from molecular simulations. *PLOS Comput. Biol.* 8:e1002605.

17. Moritsugu, K., T. Terada, and A. Kidera. 2012. Disorder-to-order transition of an intrinsically disordered region of sortase revealed by multiscale enhanced sampling. *J. Am. Chem. Soc.* 134:7094–7101.

18. Zhang, W. H., and J. H. Chen. 2014. Accelerate sampling in atomistic energy landscapes using topology-based coarse-grained models. *J. Chem. Theory Comput.* 10:918–923.

19. Liu, P., B. Kim, …, B. J. Berne. 2005. Replica exchange with solute tempering: a method for sampling biological systems in explicit water. *Proc. Natl. Acad. Sci. USA.* 102:13749–13754.

20. Wang, L., R. A. Friesner, and B. J. Berne. 2011. Replica exchange with solute scaling: a more efficient version of replica exchange with solute tempering (REST2). *J. Phys. Chem. B.* 115:9431–9438.

21. Terakawa, T., T. Kameda, and S. Takada. 2011. On easy implementation of a variant of the replica exchange with solute tempering in GROMACS. *J. Comput. Chem.* 32:1228–1234.

22. Bussi, G. 2014. Hamiltonian replica exchange in GROMACS: a flexible implementation. *Mol. Phys.* 112:379–384.

23. Miller, C. M., A. C. Brown, and J. Mittal. 2014. Disorder in cholesterol-binding functionality of CRAC peptides: a molecular dynamics study. *J. Phys. Chem. B.* 118:13169–13174.

24. Huang, K., and A. E. García. 2014. Acceleration of lateral equilibration in mixed lipid bilayers using replica exchange with solute tempering. *J. Chem. Theory Comput.* 10:4264–4272.

25. Cole, D. J., J. Tirado-Rives, and W. L. Jorgensen. 2015. Molecular dynamics and Monte Carlo simulations for protein-ligand binding and inhibitor design. *Biochim. Biophys. Acta.* 1850:966–971.

26. Pronk, S., S. Páll, …, E. Lindahl. 2013. GROMACS 4.5: a high-throughput and highly parallel open source molecular simulation tool-kit. *Bioinformatics.* 29:845–854.

27. Hornak, V., R. Abel, …, C. Simmerling. 2006. Comparison of multiple AMBER force fields and development of improved protein backbone parameters. *Proteins.* 65:712–725.

28. Darden, T., D. York, and L. Pedersen. 1993. Particle mesh Ewald—an NLog(N) method for Ewald sums in large systems. *J. Chem. Phys.* 98:10089–10092.

29. Hess, B., H. Bekker, …, J. G. E. M. Fraaije. 1997. LINCS: a linear constraint solver for molecular simulations. *J. Comput. Chem.* 18:1463–1472.

30. Shen, Y., and A. Bax. 2010. SPARTA+: a modest improvement in empirical NMR chemical shift prediction by means of an artificial neural network. *J. Biomol. NMR.* 48:13–22.

31. Race, P. R., M. L. Bentley, …, M. J. Banfield. 2009. Crystal structure of *Streptococcus pyogenes* sortase A: implications for sortase mechanism. *J. Biol. Chem.* 284:6924–6933.

32. Guo, J., and H. X. Zhou. 2015. Dynamically driven protein allostery exhibits disparate responses for fast and slow motions. *Biophys. J.* 108:2771–2774.

33. Patriksson, A., and D. van der Spoel. 2008. A temperature predictor for parallel tempering simulations. *Phys. Chem. Chem. Phys.* 10:2073–2077.

34. Cascioferro, S., M. Totsika, and D. Schillaci. 2014. Sortase A: an ideal target for anti-virulence drug development. *Microb. Pathog.* 77:105–112.

35. Chan, A. H., J. Wereszczynski, …, R. T. Clubb. 2013. Discovery of *Staphylococcus aureus* sortase A inhibitors using virtual screening and the relaxed complex scheme. *Chem. Biol. Drug Des.* 82:418–428.

36. Krebs, W. G., and M. Gerstein. 2000. The Morph server: a standardized system for analyzing and visualizing macromolecular motions in a database framework. *Nucleic Acids Res.* 28:1665–1675.

Disorder-to-order transition of an active-site loop mediates the allosteric activation of sortase A

Xiaodong Pang and Huan-Xiang Zhou*

Department of Physics and Institute of Molecular Biophysics, Florida State University, Tallahassee, FL 32306
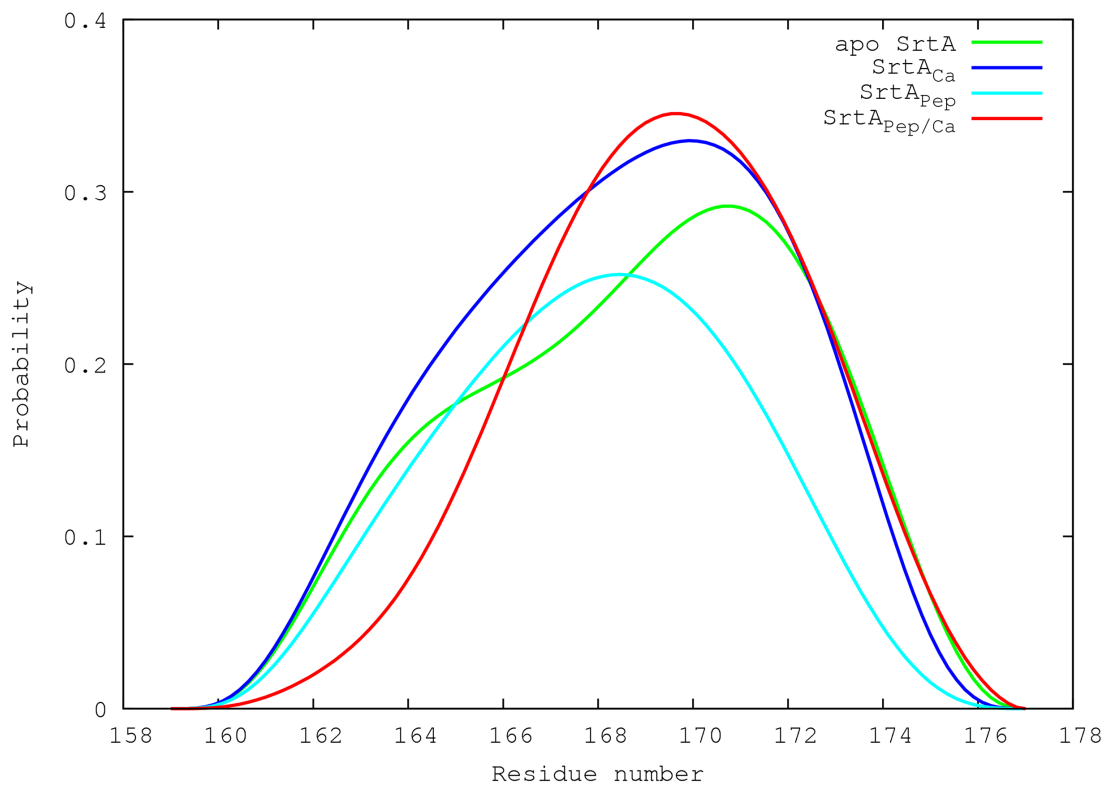
SUPPORTING MATERIAL

Figure S1 Distributions of the probabilities of residues in the active-site loop for forming 3_{10} helix, obtained from the REST simulations on sortase A in the apo form and in the three liganded forms.
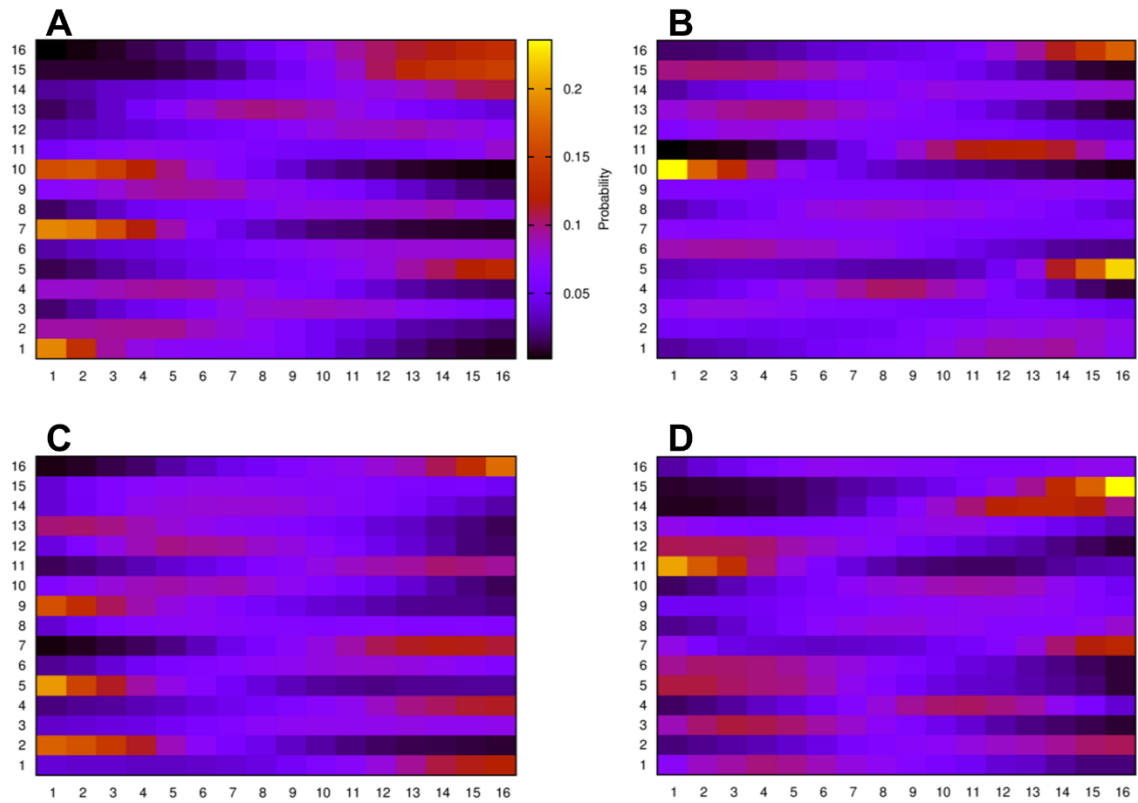
Figure S2 Probabilities of each replica, started from a particular position along the temperature ladder, to be at all the 16 positions in the ladder during the 100-ns simulations. The vertical axis indicates the starting position. (A) Apo SrtA. (B) $SrtA_{Ca}$. (C) $StrA_{Pep}$. (D) $StrA_{Pep/Ca}$.
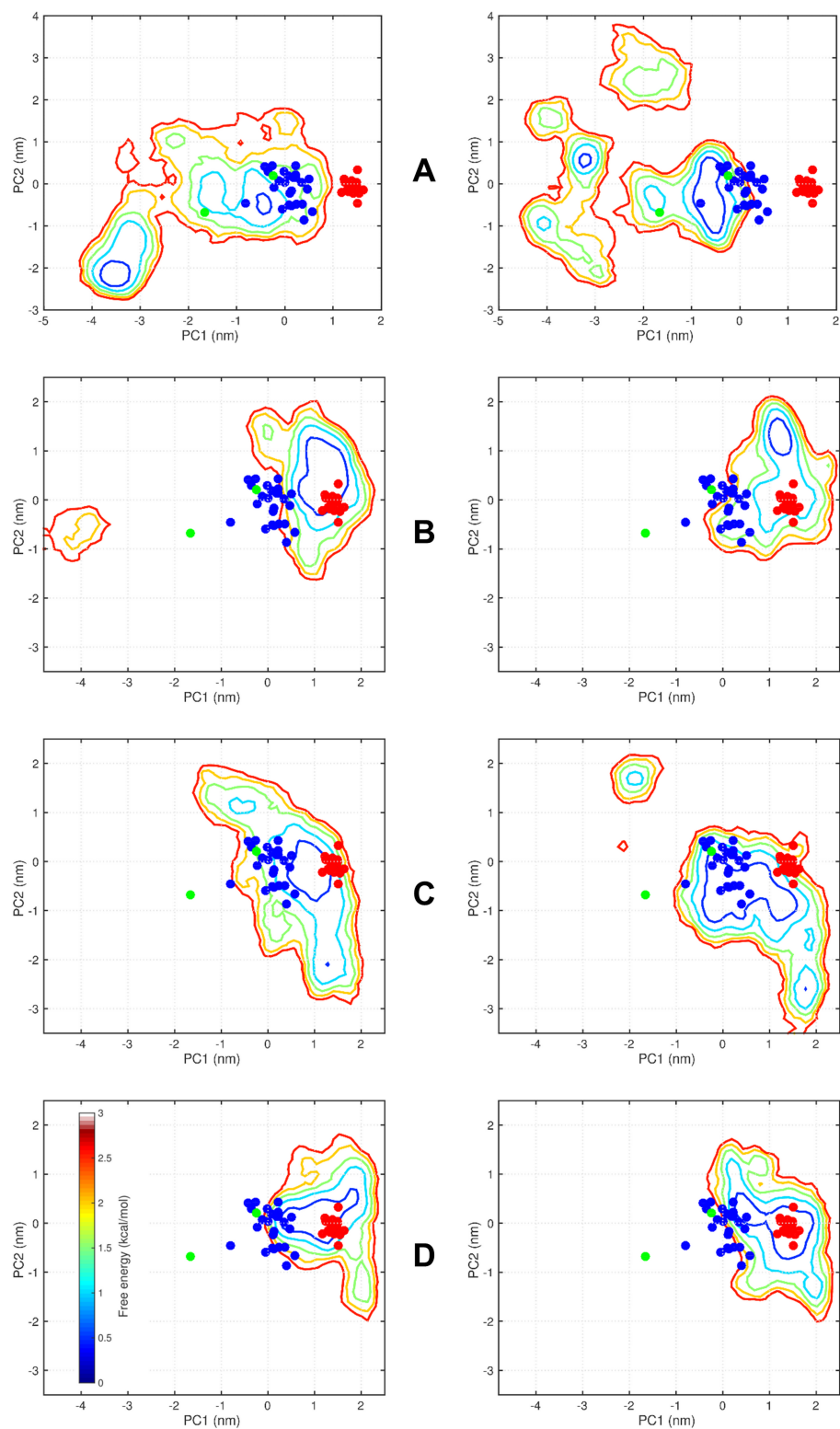
Figure S3 Conformational ensembles of the four forms of SrtA. (A) Apo. (B) SrtA$_{Ca}$. (C) StrA$_{Pep}$. (D) StrA$_{Pep/Ca}$. Left and right panels display results calculated from 0-50 ns and 50-100 ns of the simulations.
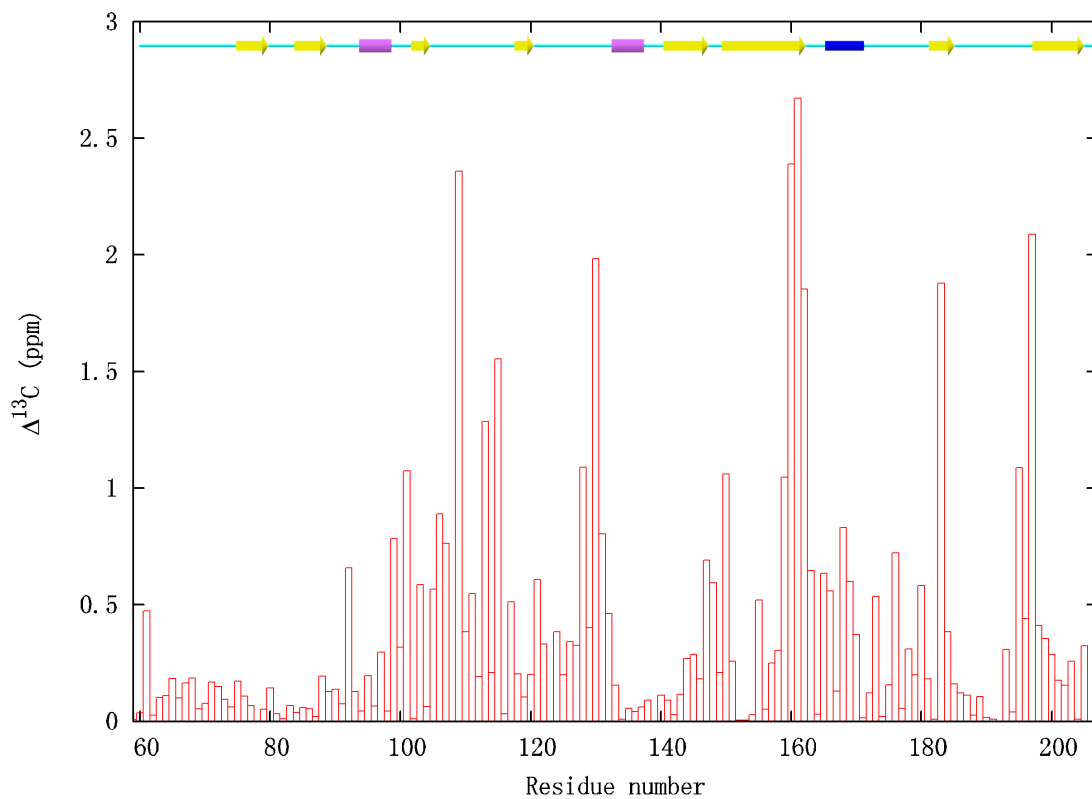
Figure S4 Predicted changes in Cα chemical shifts of sortase A upon Ca^{2+} binding. The secondary structure of the protein is shown at the top.